ACERP: Vol. 4, No. 3 & 4, (Summer & Fall 2018) 43-49

Advanced Ceramics Progress

Research Article

Journal Homepage: www.acerp.ir

An investigation on the effect of acetone and DMF as solvent on synthesis of P_2O_5-CaO-Na_2O-TiO_2 glass powder by sol-gel method

Marzieh Jalilpour[1], Mohammad Rezvani*[1], Khalil Farhadi[2]

[1] *Department of Materials Science and Ceramics, University of Tabriz, Tabriz, Iran*
[2] *Faculty of Chemistry of Urmia University, Urmia, Iran*

PAPER INFO

Paper history:

Received 19 June 2019
Accepted in revised form 09 July 2019

Keywords:

Phosphate-based glass
Sol-gel
Acetone
Dimethylformamide
SBF

ABSTRACT

The sol-gel synthesis method allows greater control over glass morphology at a relatively low processing temperature (200 °C) in comparison with melt-derived glasses. In present study, phosphate-based glasses with the general formula of $(P_2O_5)_{55}$-$(CaO)_{25}$-$(Na_2O)_{10}$-$(TiO_2)_{10}$ was synthesized via a novel and facile sol-gel method for use in biomedical applications. For this purpose, dimethylformamide and acetone were used as the solvent. Glass powders that are obtained from the dried gel was analyzed using several characterization techniques including X-Ray Diffraction, Fourier Transform Infrared Spectroscopy, Simultaneous Thermal Analysis, Brunauer-Emmett-Teller surface area and porosity analyzer and Scanning Electron Microscopy. The X-Ray Diffraction results confirmed the amorphous and glassy nature of prepared samples. The Fourier Transform Infrared spectroscopy results revealed that by adding TiO2, titanium oxide (TiO_6) entered into the network which likely acts as an oxide modifier. It was observed that crystallization temperature (T_c) for the sample synthesized by dimethylformamide (DMF) (~646 °C) is more than the one synthesized by acetone (~500 °C). The surface area of the acetone and DMF of synthesized samples is 40 m^2/g and 44.5 m^2/g, respectively. Furthermore, to examine the bioactive capacity of glasses, the samples were soaked in a simulated body fluid (SBF) for 7 days. The analyses were shown the formation of hydroxyapatite on glass powders after 7 days of immersion in SBF solution. The morphology of hydroxyapatite was spherical and its particle size was ~8 nm.

1. INTRODUCTION

Bioactive glasses (BG) are inorganic ones that because of their good bioactivity, osteoconductivity and biodegradability have many applications in the biomedical engineering [1]. They promote bone/tissue formation at their surface and bond to living tissue without the establishment of fibrous tissue around them [2].

Among various bioactive glass systems, bioresorbable materials can be resorbed in the body and replaced by bone and tissue cells. In comparison with metallic implants which may exhibit complications such as tissue irritation and inflammation that may require secondary surgery to remove the implant, resorbable materials are offered a potential solution to these problems by eliminating the need for follow up surgery in order to remove the implant [3].

In recent years, there has been several papers on improving the physical properties and chemical durability of phosphate glasses by adding different metal oxides with high valency cations such as Ti^{4+}, Fe^{3+}, Al^{3+}, Cu^{2+}, Zn^{2+}, etc. because of the formation of relatively stable cross-linked bonds in the phosphate network [4-9]. Phosphate-based glasses have a variety of interesting properties which make them suitable for biomedical applications composing of bone cavity fillers, drug delivery systems, biodegradable reinforcing phase in the case of composites for bone fixation devices and tissue engineering scaffolds [10]. This type of glasses containing Ca^{2+} and Na^{+} ions has desirable properties for drug delivery applications. For several years, such glass has been utilized as passive host materials for the

* *Corresponding Author Email: m_rezvani@tabrizu.ac.ir (M. Rezvani)*

controlled release of metal ions in a variety of applications including veterinary treatments [11] and antibacterial ingredients [12]. It is biocompatible and bioresorbable that has near linear dissolution rate in aqueous media. Moreover, the degradation rate can be finely tuned through subtle variations in the composition [13]. Linear dissolution is particularly important because one of the common problems associated polymer-based drug delivery devices is an 'initial burst' of release that is followed by a much lower release rate. Biocompatibility may also offer a significant advantage over the current polymer-based systems where their degradation can result in polymer fragments with heterogeneous chain-lengths which can lead to toxicity. Until now, using the phosphate-based glass in drug delivery devices has been limited by the high temperatures required in their preparation and quenching a melt consisting of oxide precursors which restricts the types of molecules that can be incorporated. Using the low-temperature sol-gel route largely circumvents this problem [14].

The sol-gel technique is an alternative approach to fabricate bioglasses that has been widely studied in recent years. The advantages of the sol-gel process are well known: the process takes place at low temperatures and gives homogeneous mixtures in the final glass composition [15].

Up to now, in phosphate-based glasses that are synthesized by the sol-gel method, very limited solvents such as 2-methoxy ethanol, deionized water and ethanol etc. have been used [16-18].

To the best of our knowledge, the synthesis of the bioactive glass via the sol-gel has not been synthesized by acetone or dimethylformamide as solvents. Therefore, in the present study, the sol-gel method was carried out for the synthesis of quaternary $55P_2O_5$-25CaO-$10Na_2O$-$10TiO_2$ bioglass powders by two various solvents. The prepared samples by acetone and N-dimethylformamide solvents were investigated by XRD, FTIR, BET-BJH and FE-SEM analytical instruments before and after soaking in SBF.

2. MATERIALS AND METHODS

2.1. MATERIALS

The following chemical precursors were used without further purification; Triethyl phosphate (Sigma Aldrich, ≥99.8%), Titanium isopropoxide (Merck, 97%), Calcium nitrate tetrahydrate (Merck, ≥99.7, %30 wt% in ethanol), sodium methoxide solution (Sigma Aldrich, ≥95 %, 30 wt% in ethanol), Ethanol (Merck, ≥99.7%), Acetone (Merck, ≥99.7%) and Dimethylformamide (DMF) (Merck, 99.8%).

2.2. SYNTHESIS OF THE GLASS POWDER

The reaction was started by diluting triethyl phosphate in the acetone and dimethylformamide in two separate dry vessels with a molar ratio of 1:3 for triethyl phosphate: acetone and 1:3 for triethyl phosphate: dimethylformamide, respectively. Then, both solutions were stirred for 15 min. At that time, titanium isopropoxide solution was added to the mixture dropwise while it was magnetically stirring. Following that, after 1h stirring, calcium nitrate tetrahydrate solution (30 wt% in ethanol) was gradually added into the vessels. Stirring was continued for 1h and then sodium ethoxide solution (30 wt% in ethanol) was added drop by drop and stirring was continued for 1h again. For all samples, the mixtures were poured into porcelain crucibles and allowed them to get gel at room temperature. The mixtures turned to gel and were aged for 3 days at room temperature.

Following the aging stage, the temperature was increased up to 60 °C and kept for 2 days, and thenthe temperature was increased up to 120 °C for 2 days, 180°C for 2 days, 200 °C for 2h and 315 °C for 2h to remove any remaining solvents and nitrate. The semi-bulk samples containing 10% TiO_2 synthesized by acetone and dimethylformamide were named Ace_{10} and Dmf_{10}, respectively. Table 1 shows the code and chemical composition of samples. Furthermore, the flowchart of synthesis is shown in Fig. 1.

2.3. CHARACTERIZATION

Powder X-ray diffraction was performed on an X-ray diffractometer (Philips PW1730, Netherland) using Cu K_α radiation (λ= 1.5406 A) and the detection range was 10-80°. Morphology of samples was investigated using field emission scanning electron microscopy (TSCAN, Mira3LMU, Czech Republic). Fourier transform infrared spectra were recorded on an infrared spectrophotometer (NEXUS 670, USA).

About 10 mg of each sample was blended with KBr for IR spectroscopy (Sigma-Aldrich) and then pressed into translucent pellets for the measurement in the range of 400-4000 cm^{-1}. Brunauer-Emmett-Teller and Barrett-Joyner-Halenda analyses were employed to determine surface area, pore size distribution and pore volume of the N_2 adsorption-desorption isotherms (BET, Belsorp mini II, USA). Differential thermal analysis (Bahr, STA 504, Germany) was conducted to identify the glass transition (T_g) and crystallization temperatures (T_c) of studied glasses. Analyses were carried out on powdered glass samples in an alumina crucible from 25 to 800 °C at a heating rate of 10 °C/min under air atmosphere. A crucible with alumina (Al_2O_3) was used as a reference. The thermogravimetric analysis (TGA) was served to quantify the total weight loss of samples.

In order to evaluate the hydroxyapatite (HA) mineralization ability of two synthesized glass nanopowders in vitro bioactivity, 1 mg of samples was ground and soaked in 25 mL SBF solution at 37.5°C for 7 days in a CO_2 incubator. The SBF solution was prepared and buffered at pH 7.4 according to the procedure reported by Kokubo [3].

TABLE 1. The compositions of glass powders

Sample code	Theoretical formulation	Concentration (mol %)				Solvent
		P_2O_5	CaO	Na_2O	TiO_2	
Ace_{10}	$55P_2O_5$-25CaO-$10Na_2O$-$10TiO_2$	55	25	10	10	Acetone
Dmf_{10}	$55P_2O_5$-25CaO-$10Na_2O$-$10TiO_2$	55	25	10	10	Dimethylformamide

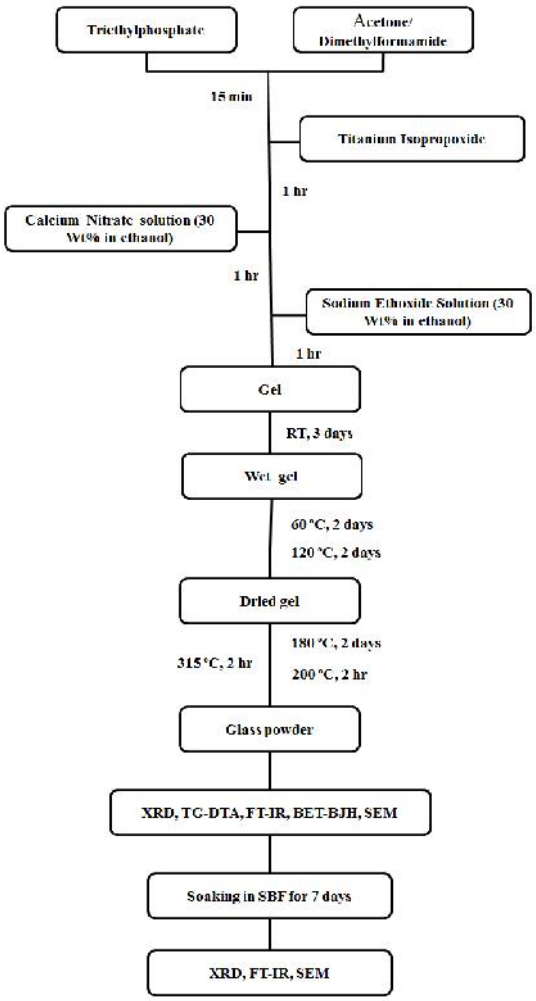

Figure 1. Flow chart of synthesizes glass powders by acetone and dimethylformamide

XRD, FTIR and FE-SEM analyses were employed to study the hydroxyapatite formation on the surface of the samples.

3. RESULT AND DISCUSSION

DTA analyzes were used to determine the glass transition (T_g) and crystallization starting temperatures (T_c) of both Ace_{10} and Dmf_{10} samples according to the onset temperature of the DTA curve (Fig. 2 (a and b)). The peaks were divided into two regions for Ace_{10}: 25-200°C and 200-800°C. In the 25-200°C region, the glass sample exhibited an endothermic peak due to the release of small amounts of physically absorbed water and crystal water (~5 wt %). At 200-800°C, the glass sample demonstrated an endothermic peak due to the release of nitrates and other solvents and two exothermic peaks because of appearance of the glass transition and crystallization at 200-800°C. The glass transition temperature and the first crystallization temperature for Ace_{10} were determined 472°C and 498°C, respectively. In this region, weight loss is about 12.5%. In addition, for Dmf_{10}, the peaks were divided into two regions: 25-200°C and 200-800°C. In the first one, a spread endothermic peak below 100°C was perceived due to the release of very small amounts of physically absorbed water and crystal water (~0.8 wt %). In the second one, a sharp endothermic peak was observed at the outgoing of nitrates and solvents at 313°C. The peaks at 537°C, 646°C and 736°C are the glass transition (T_g), the first (T_{c1}) and second (T_{c2}) crystallization temperatures in that order. As can be seen, the glass transition temperature of the Ace_{10} sample about 63°C is less than the temperature of the Dmf_{10} sample, while the crystallization temperature of Ace_{10} is 148°C less than the Dmf_{10}'s.

Figure 3 shows the XRD patterns of two sol-gel glass samples synthesized by acetone and dimethylformamide before and after 7 days soaking in SBF. For two samples, before soaking in SBF, a broad peak at 2θ values between 10° and 80° was observed and was free from any detectable crystalline phase, confirming the amorphous and glassy nature of prepared samples. But, as seen after 7 days soaking in SBF, the sharp peaks assigning to hydroxyapatite (ICDD - PDF2 card: 00-009-0432) appear [19].

The FT-IR spectra of the Ace_{10} and Dmf_{10} glass samples, before and after soaking in SBF are shown in Fig. 4. The absorption bands were assigned according to other studies of phosphate-based glasses using infrared spectroscopy [20-22].

The spectra from the sol-gel samples display the bands characteristic of P-O-P bonding at ~550-580 cm^{-1} and ~740 cm^{-1}, indicating a significant number of bonds were formed during the sol-gel reaction. The asymmetric $(PO_3)^{-2}$ stretching modes at ~987 cm^{-1} and 1116 cm^{-1} $(PO_4)^{-3}$ and the band near 1250 cm^{-1} were assigned to the asymmetric stretching mode of $(PO_2)^-$. The bands at ~3420 and 1640 cm^{-1} are due to the presence of hydroxyl groups and adsorbed moisture [23].The FT-IR spectra of

samples after 7 days soaking in SBF present a relatively sharp stretching band derived from hydroxyl ions which was clearly observed at 3415-3430 cm^{-1}.

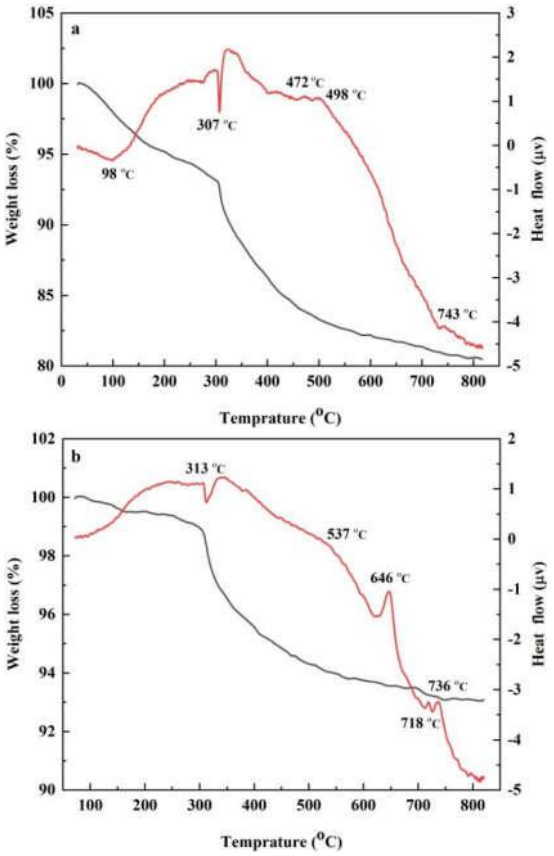

Figure 2. Simultaneous TGA and DTA measurements of the a) Ace_{10} and b) Dmf_{10} glass powder

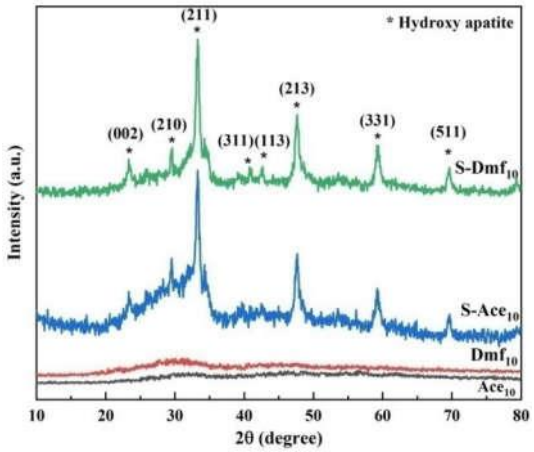

Figure 3. XRD spectra of sol-gel derived glasses containing 10 % mol TiO_2, synthesized with acetone and DMF before and after 7 days soaking in SBF

Additionally, the bending mode band at ~1649 cm^{-1} from H_2O was also observed in the spectrum as usual for precipitated coatings. Some small bands associated with C-H stretching mode were observed at ~2190 cm^{-1} and 2338-2345 cm^{-1} which indicate the presence of some residual organic material [23].

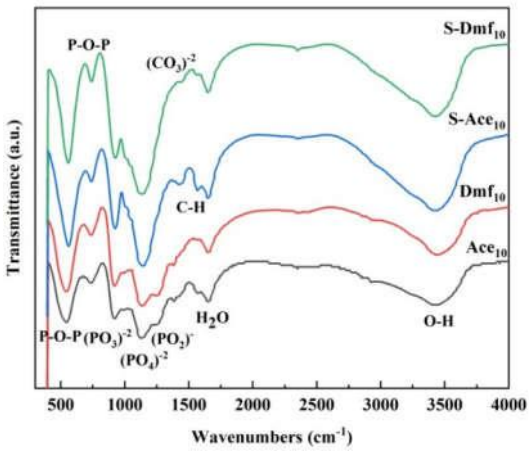

Figure 4. FT-IR spectra of Ace_{10} and Dmf_{10} glass powders before and after 7 days soaking in SBF

A phosphate band derived from the P-O asymmetric stretching mode of the $(PO_3)^{-2}$ group were found in the region from 1133 to 1149 cm^{-1}. Moreover, the other small bands at 1041 and 1056 cm^{-1} were associated with symmetric stretching $(PO_3)^{-2}$ and asymmetric stretching mode of the $(PO_4)^{-3}$ [21, 23]. The bands at 1438 cm^{-1}, 1445 cm^{-1}, and 1452 cm^{-1} from the $(CO_3)^{-2}$ group of carbonated apatite were difficult to assign indicating that the content of $(CO_3)^{-2}$ is low [24]. However, the characteristic peaks at 920 cm^{-1} could indicate the presence of HPO_4^{-2} in the crystal lattice [24]. The band at 739 cm^{-1} and ~559-574 cm^{-1} could be associated with P-O-P symmetric and asymmetric stretching band, respectively. The results indicated that the Ca/P deposit is most likely formed by an appetite with low content of carbonate so that the presence of HPO_4^{-2} could indicate a deficiency of calcium in the newly formed coating [23, 24].

Specific surface area, average pore diameter, and total pore volume of Ace_{10} and Dmf_{10} were measured and the values are summarized in Table 2. The samples were degassed at 200°C for a period of 2 h in flowing nitrogen doing making the BET-BJH measurements. The adsorption isotherm and pore distribution diagram of Dmf_{10} and Ace_{10} samples are shown in Fig. 5 (a-d). The specific surface area obtained from the adsorption isotherms is ~40 m^2/g for Ace_{10} and ~44.5 m^2/g for Dmf_{10}.

The adsorption isotherm curves of samples were identified as type IV and II isotherms for Ace_{10} and Dmf_{10}, respectively. These isotherms are characteristic of

mesoporous materials. Consequently, it can be argued that the adsorption in Ace_{10} is multilayer whereas in Dmf_{10} is pore filling which is followed by outer-surface adsorption [25].

The hysteresis loop is H_1 type for Ace_{10} and H_3 type for Dmf_{10} in the mesopore range. The H_1 is characteristic of cylindrical pores open on both sides and H_3 is related to slit-shaped pores, too [25]. Correspondingly, it is clear that the pore diameter distribution in the Ace_{10} sample is very ordered and uniform, whereas in the pore diameter distribution of the Dmf_{10} sample is widespread [25]. Furthermore, Dmf_{10} has a smaller peak pore diameter than Ace_{10} (Fig. 5 (c and d)).

TABLE 2. Specific surface area, average pore diameter and total pore volume of Ace_{10} and Dmf_{10}

Sample name	Ace_{10}	Dmf_{10}
specific surface area (m^2/g)	40.04	44.47
total pore volume (cm^3/g)	0.2050	0.2860
average pore diameter (nm)	20.477	25.721
peak pore diameter (nm)	9.19	1.21

SEM images of produced Ace_{10} and Dmf_{10} bioactive glass nanopowders, before and after 7 days soaking in SBF are shown in Fig. 6 (a-d).

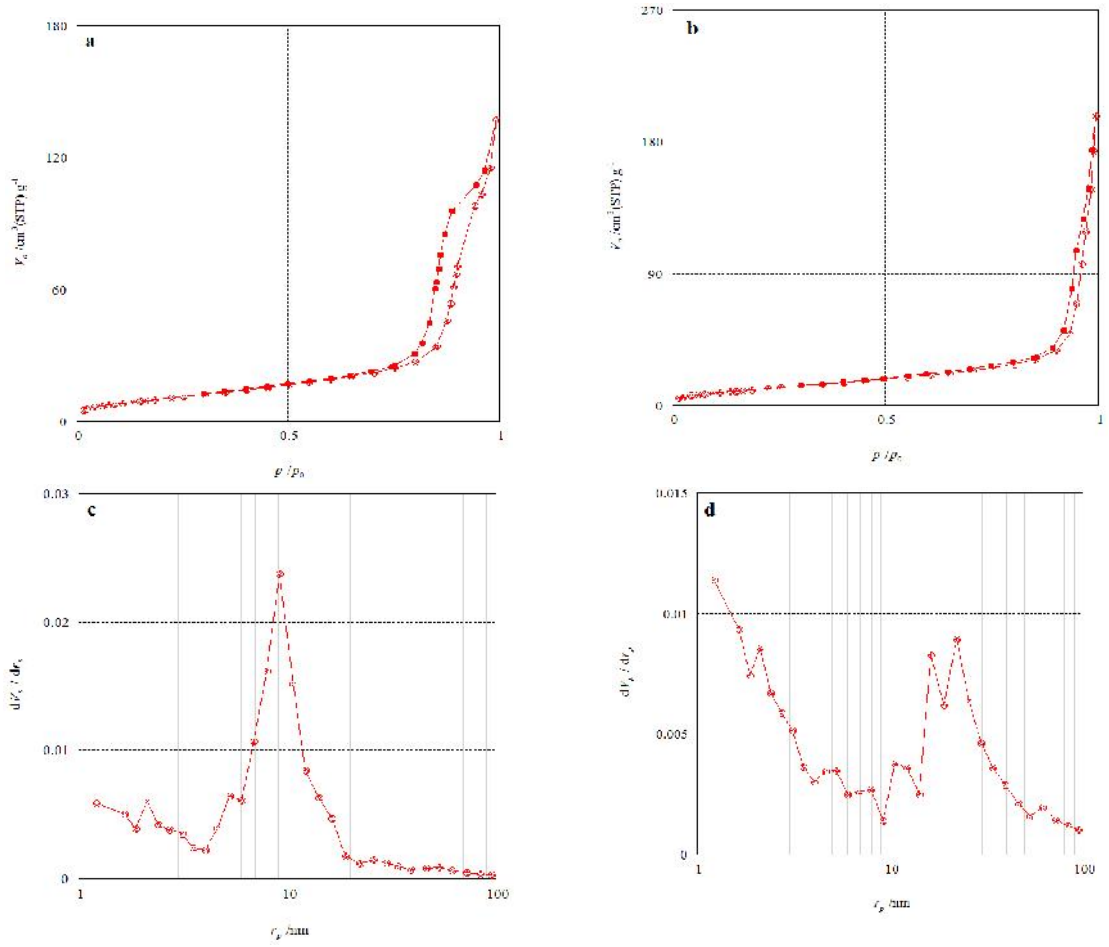

Figure 5. Adsorption isotherm, a) Ace_{10}, b) Dmf_{10} and pore distribution diagram, c) Ace_{10}, d) Dmf_{10}

These figures are used for the study of the size, morphology, and homogeneity of glass nanopowders. As seen in these figures, it is interesting to see that all particles are spherical and their size is below 50 nm. Mean particle size of glass powders before soaking in SBF are ~20 nm and ~22 nm for Ace_{10} and Dmf_{10}, respectively (Fig. 6(a and b)). As be seen, severe agglomeration was observed in both glass powders because of the very small size of them. It can be related to the properties of the sol-gel method that the bioglass synthesized from it. Figure 6 (c and d) shows the surface of the samples after soaking in SBF solution. Compared

to Fig. 6(a and b), it can be clearly seen that in these samples, apatite particles formed on the surface after soaking in SBF (as shown in XRD and FT-IR results). The mean particle size of hydroxyapatite particles is ~8 nm for both samples. Besides, the morphology of the formed hydroxyapatite is spherical.

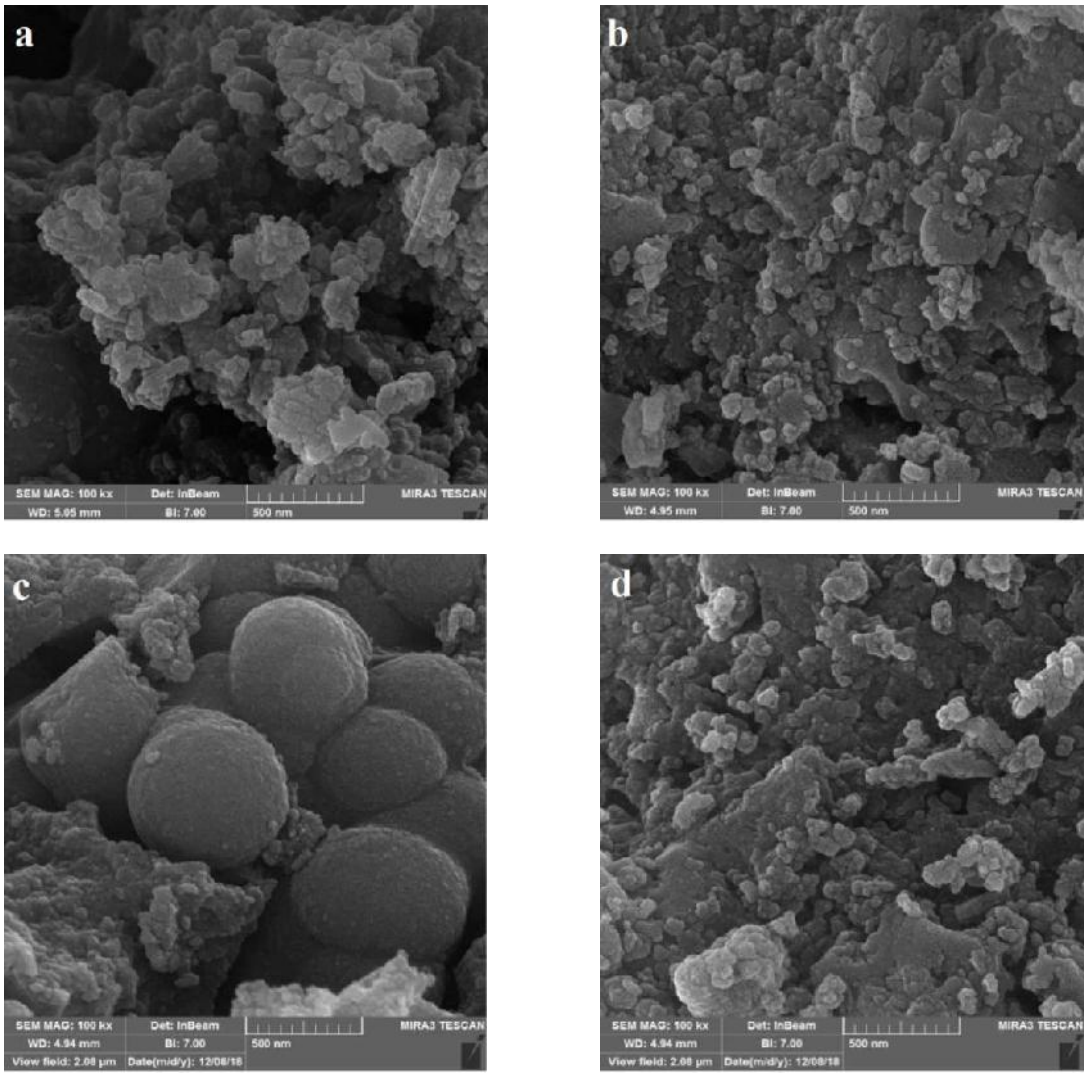

Figure 6. SEM images of glass powder before soaking in SBF, a) Ace_{10}, b) Dmf_{10}, after soaking in SBF for 7 days, c) Ace_{10}, d) Dmf_{10}

4. CONCLUSION

In this study, the effect of two different solvents on the properties of phosphate-based glass powders synthesized by the sol-gel method was investigated. The results showed that both solvents cause the formation of amorphous glass powders with spherical morphology. The relatively good surface area was achieved for both glass nanopowders to use in the biomedical. The immersion in the simulated body fluid for 7 days revealed the bioactive ability of both samples. On the surface of glasses, the spherical hydroxyapatite coating was formed with ~8 nm diameter.

5. ACKNOWLEDGMENT

The authors would like to thanks for the support of the Institute of nanotechnology and biotech center of Urmia University for this research.

REFERENCES

1. Solgi, S., Khakbiz, M., Shahrezaee, M., Zamanian, A., Tahriri, M., Keshtkari, S., Raz, M., Khoshroo, K., Moghadas, S., Rajabnejad, A., "Synthesis, Characterization and In Vitro Biological Evaluation of Sol-gel Derived Sr-containing Nano Bioactive Glass", ***Silicon***, Vol. 9, No. 5, (2017), 535-542.
2. Syed Nuzul Fadzli, S. A., Roslinda, S., Zainuddin, F., Ismail, H., "Synthesis of sol-gel derived glass powder and in vitro bioactivity property tested in simulated body fluid", ***AIP Conference Proceedings***, Vol. 1784, No. 1, (2016), 1-5.
3. 3. Foroutan, F., De Leeuw, N. H., Martin, R. A., Palmer, G., Owens, G. J., Kim, H. W., Knowles, J. C., "Novel sol-gel preparation of $(P_2O_5)_{0.4}$ - $(CaO)_{0.25}$ - $(Na_2O)_X$ - $(TiO_2)_{(0.35-X)}$ bioresorbable glasses (X = 0.05, 0.1, and 0.15)", ***Journal of Sol-Gel Science Technology***, Vol. 73, No. 2, (2015), 434-442.
4. Minami, T., Mackenzie, J. D., "Thermal-expansion and chemical durability of phosphate glasses", ***Journal of American Ceramic Society***, Vol. 60, (1977), 232-235.
5. Lakhkar, N., Abou Neel, E. A., Salih, V., Knowles, J. C., "Titanium and strontium-doped phosphate glasses as vehicles for strontium ion delivery to cells", ***Journal of Biomaterial Applications***, Vol. 25, (2011), 877-893.
6. Banijamali, S., Eftekhari Yekta, B., Aghaei, A.R., "Self-patterning of porosities in the $CaO-Al_2O_3-TiO_2-P_2O_5$ glass-ceramics via ion exchange and acid leaching process", ***Journal of Non-Crystalline Solids***, Vol. 380, (2013), 114-122.
7. Islam, M. T., Felfel, R. M., Abou Neel, E. A., Grant, D. M., Ahmed, I., Zakir Hossain, K. M., "Bioactive calcium phosphate-based glasses and ceramics and their biomedical applications: A review", ***Journal of Tissue Engineering***, Vol. 8, (2017), 1-16.
8. Kiani, A., Hanna, J. V., King, S. P., Rees, G. J., Smith, M. E., Roohpour, N., Salih, V., Knowles, J. C., "Structural characterization and physical properties of P_2O_5-CaO-Na_2O-TiO_2 glasses by Fourier transform infrared, Raman and solid-state magic angle spinning nuclear magnetic resonance spectroscopies", ***Acta Biomaterialia***, Vol. 8, (2012), 333-340.
9. Fernandes, J. S., Gentile, P., Pires, R. A., Reis, R. L., Hatton, P. V., "Multifunctional bioactive glass and glass-ceramic biomaterials with antibacterial properties for repair and regeneration of bone tissue", ***Acta Biomaterialia***, Vol. 1, No.59, (2017), 2-11.
10. Pickup, D. M., Wetherall, K. M., Knowles, J. C., Smith, M. E., Newport, R. J., "Sol-gel preparation and high-energy XRD study of $(CaO)_x(TiO_2)_{0.5-x}(P_2O_5)_{0.5}$ glasses (x = 0 and 0.25)", ***Journal of materials science materials in medicine***, Vol. 19, (2008), 1661-1668.
11. Rehr, J. J., Albers, R. C., Zabinsky, S. I., "High-order multiple-scattering calculations of x-ray-absorption fine structure", *Physical review letters*, Vol. 69, No. 23, (1992), 3397.
12. Fletcher, D. A., Mc Meeking, R. F., Parkin, D., "The United Kingdom chemical database service", ***Journal of Chemical Information and Computer Sciences***, Vol. 36, (1996), 746-749.
13. Cole, J. M., van Eck, E.R. H., Mountjoy, G., Anderson, R., Brennan, T., Bushnell-Wye, G., Newport, R. J., Saunders, G. A., "An x-ray diffraction and ^{31}P MAS NMR study of rare-earth phosphate glasses, $(R_2O_3)x(P_2O_5)_{1-}x$, x = 0.175-0.263, R =La, Ce, Pr, Nd, Sm, Eu, Gd, Tb, Dy, Ho, Er", ***Journal of Physics: Condensed Materials***, 13, (2001), 4105-4122.
14. Pickup, D. M., Valappil, S. P., Moss, R. M., Twyman, H. L., Guerry, P., Smith, M. E., Wilson, M., Knowles, J. C., Newport, R. J., "Preparation, structural characterisation and antibacterial properties of Ga-doped sol-gel phosphate-based glass", ***Journal of Materials Science***, Vol. 44, No. 7, (2009), 1858-1867.
15. Abou Neel, E. A., A. O'Dell, L., Smith, M. E., Knoweles, J. C., "Processing, characterization, and biocompatibility of zinc modified metaphosphate based glasses for biomedical applications", ***Journal of Materials Science. Materials in Medicine***, Vol. 19, No. 4, (2008), 1669-1679.
16. Foroutan, F., De Leeuw, N. H., Martin, R. A., Palmer, G., Owens, G. J., Kim, H. W., Knowles, J. C., "Novel sol-gel preparation of $(P_2O_5)_{0.4}$-$(CaO)_{0.25}$-$(Na_2O)_X$-$(TiO_2)_{(0.35-X)}$ bioresorbable glasses (X = 0.05, 0.1, and 0.15)", ***Journal of Sol-Gel Science and Technology***, Vol. 73, No. 2, (2014), 434-442.
17. Soulié, J., Gras, P., Marsan, O., Laurencin, D., Rey, C., Combes, C., "Development of a new family of monolithic calcium (pyro) phosphate glasses by soft chemistry", ***Acta Biomaterialia***, Vol. 41, (2016), 320-327.
18. Muthusamy, P., Kandiah, K., Manivasakan, P., Venkatachalam, R., "In Vitro Bioactivity and Antimicrobial Tuning of Bioactive Glass Nanoparticles Added with Neem (Azadirachta indica) Leaf Powder", ***Journal of Biomedicine and Biotechnology***, Vol. 11, No. 950691, (2014), 1-10.
19. Ungureanu, D. N., Angelescu, N., Bacinschi, Z., Valentina Stoian, E., Rizescu, C. Z., "Thermal stability of chemically precipitated hydroxyapatite nanopowders", ***International Journal of Biology and Biomedical Engineering***, Vol. 5, No. 2, (2011), 57-64.
20. Kim, D. S., Shin, J. Y., Ryu, B. K., "Proton Conduction in and Structure of P_2O_5-TiO_2-CaO-Na_2O Sol-Gel Glasses", ***Journal of the Korean Physical Society***, Vol. 70, No.12, (2017), 1054-1059.
21. Arsad Maisara, S. M., Pat, M. L., "Synthesis and Characterization of hydroxyapatite Nanoparticles and β-TCP Particles", ***2nd International Conference on Biotechnology and Food Science***, Vol. 7, (2011), 184-188.
22. Davim, E. J. C., Fernandes, M. H. V., Senos, A. M. R., "Increased surface area during sintering of calcium phosphate glass and sodium chloride mixtures", ***Journal of the European Ceramic Society***, Vol. 35, (2015), 329-336.
23. Pickup, D. M., Guerry, P., Moss, R. M., Knowles, J. C., Smith, M. E., Newport, R. J., "New sol-gel synthesis of a $(CaO)_{0.3}(Na_2O)_{0.2}(P_2O_5)_{0.5}$ bioresorbable glass and its structural characterization", ***Journal of Materials Chemistry***, Vol. 17, (2007), 4777-4784.
24. Alonso, L. M., Garcıa-Menocal, J. A. D., Aymerich, M. T., Guichard, J. A. A., Garcıa-Valles, M., Manent, S. M., Ginebra, M., "Calcium phosphate glasses: Silanation process and effect on the bioactivity behavior of Glass-PMMA composites", ***Journal of biomedical materials research B: applied biomaterials***, Vol. 00B, (2013), 1-9.
25. Montazerian, M., Eftekhari Yekta, B., Marghussian, V. K., Bellani, C. F., Siqueira, R. L., Zanotto, E. D., "Bioactivity and cell proliferation in radiopaque gel-derived $CaO-P_2O_5-SiO_2-ZrO_2$ glass and glass-ceramic powders", ***Materials Science and Engineering C***, Vol. 55, (2015), 436-447.